Journal of King Saud University – Science 34 (2022) 101841

Contents lists available at ScienceDirect

Journal of King Saud University – Science

journal homepage: www.sciencedirect.com

Original article

Sunlight assisted photocatalytic dye degradation using zinc and iron based mixed metal-oxides nanopowders

Muhammad Tariq Saeed Chani [a,b,*], Sher Bahadar Khan [a,b], Mohammed M. Rahman [a,b], Tahseen Kamal [a,b], Abdullah M. Asiri [a,b]

[a] Center of Excellence for Advanced Materials Research, King Abdulaziz University, Jeddah 21589, P.O. Box 80203, Saudi Arabia
[b] Chemistry Department, Faculty of Science, King Abdulaziz University, Jeddah 21589, P.O. Box 80203, Saudi Arabia

ARTICLE INFO

Article history:
Received 25 November 2021
Revised 30 December 2021
Accepted 14 January 2022
Available online 21 January 2022

Keywords:
Low temperature synthesis
Photo-catalytic purification
Materials characterization
Water pollutants
Sunlight
Water filter

ABSTRACT

For the photocatalytic degradation of the organic dyes present in wastewater, the ternary composites of metal-oxides nanopowders of zinc-iron-calcium (Zn-Fe-Ca), zinc-iron-antimony (Zn-Fe-Sb), zinc-iron-titanium (Zn-Fe-Ti) and zinc-iron-cobalt (Zn-Fe-Co) were synthesized and characterized by different instruments. The average particle size of the Zn-Fe-Ca and Zn-Fe-Ti mixed-oxides nanopowders was 10 ± 5 nm and that of Zn-Fe-Sb nanopowder was 20 ± 10 nm. The flakes of Zn-Fe-Co nanopowder were 10 ± 5 nm thick and 100 nm to 300 nm long. All the mixed-oxides were utilized for photocatalytic degradation of acridine orange (AO) where Zn-Fe-Sb degraded the 98 % of acridine orange (AO), within 20 min, while the same level of degradation was attained by Zn-Fe-Ti and Zn-Fe-Ca mixed-oxides in 80 min and 90 min, respectively. The more efficient Zn-Fe-Sb photocatalyst was further utilized for the degradation of malachite green (MG), brilliant green (BG), methyl orange (MO) and congo red (CR). Zn-Fe-Sb was found to be fast and efficient photocatalyst for the degradation of AO and therefore, the effect of various parameters was studied in detail to optimize the reaction conditions. Moreover, the Zn-Fe-Sb mixed-oxides were used to photodegrade the AO dye in four different environmental water samples (sea, tap and sewage). Keeping in view the practical conditions, a tube-type and funnel-type filters were designed for dynamic purification process using Zn-Fe-Sb mixed-oxides as catalyst under sunlight. The synthesized nanomaterials have great potential to contribute in the wastewater treatment technologies.

1. Introduction

Water which contains bacteria, organic pollutants, industrial effluent, microorganism or any compounds which worsens its original quality is called the wastewater. The wastewater normally consists of the discharges of industrial, domestic and agricultural sources and it contains extremely toxic, non-degradable and carcinogenic contaminants like dioxin, dyes, nitroaromatics, 1,2-dichlorobenzene and heavy metal ions that may cause accumulative poisoning, nervous system damage and cancer (Ong et al., 2010). So, the world is highly concerned about water pollution and this problem can be controlled by wastewater treatment using low cost and environmental friendly processing techniques (Ong et al., 2010; Rajasulochana and Preethy, 2016; Savage and Diallo, 2005). There are many effective processes for the treatment of wastewater such as carbon adsorption, chemical precipitation, evaporations, ion exchange, membrane, photocatalysis and the biological treatment (Rajasulochana and Preethy, 2016). Out of these processes photocatalysis is one of the viable and commonly investigated process, which is very effective for the elimination of dyes, pharmaceuticals, paper industry wastes, petrochemicals and inorganic pollutants from wastewater (Rajeev et al., 2015; Rauf and Ashraf, 2009; Matthews, 1986; Lu and Pichat, 2013; Ollis et al., 2010). The beauty of the photocatalysis is its potential to use sunlight as a source of energy for wastewater treatment instead of using expensive reductants or oxidants (Ali et al., 2018; Kamal et al., 2019; Khan et al., 2019; Khan et al., 2019). Unlike to conventional wastewater treatment processes the photo-

* Corresponding author at: Office no. 576, Building no. 115, Center of Excellence for Advanced Materials Research, King Abdulaziz University, Jeddah 21589, P.O. Box 80203, Saudi Arabia.
E-mail address: mtmohamad@kau.edu.sa (M.T.S. Chani).
Peer review under responsibility of King Saud University.

Production and hosting by Elsevier

https://doi.org/10.1016/j.jksus.2022.101841
1018-3647/

catalysis process results in the complete mineralization of the pollutant into harmless products like salts, CO_2 and H_2O in ambient environment (Rajeev et al., 2015).

During the last few decades the extensive research has been conducted on semiconducting nanoparticles (SNs), which have novel electrical, electronic, semiconducting, catalytic and optical properties (Ali et al., 2018; Kasinathan et al., 2016; Kaviyarasu et al., 2020; Rathnakumar et al., 2019; Panimalar et al., 2020). Due to these properties the nanomaterials found applications in the field of sensors, light-emitting diodes, photodetectors, solar cells, switches and catalysis. Because of their high photosensitivity and efficient charge carrying capacity the SNs have become very attractive for pollutants degradation. Famous environmentally hazardous pollutants are different synthetic dyes such as congo red (CR), acridine orange (AO), malachite green (MG), brilliant green (BG) and methyl orange (MO) are the cationic dyes which are used for various purposes (Khan et al., 2016). Most of these dyes are toxic and must be eliminated from wastewater to safeguard the living organisms.

Due to their extremely small size, the nanomaterials have many folds high surface-to-volume ratio as compared to the bulk materials. This high surface-to-volume ratio is the reason for the high activity of nanomaterials, which makes them attractive for the researchers (Khan et al., 2019; Cheng et al., 2014). As a catalyst the nanomaterials are very popular in various chemical reactions such as hydrogen oxidation, hydrogen liberation, reduction reaction(Ali et al., 2017; Kamal et al., 2019), photocatalytic degradation (Rahman et al., 2017), ring opening and application in various fields such as sensing drug delivery and bio-sensing (Ali et al., 2018).

As for as the photocatalysis is concerned the semiconducting titanium oxide (TiO_2) is the extensively used catalyst for the decontamination of water and air. The advantage of ZnO over the TiO_2 is that the ZnO has wide range of absorption in the solar spectrum, while the TiO_2 absorbs in UV region only (Lam et al., 2012; Pare et al., 2008; Sakthivel et al., 2003). Due to its low cost and wide band gap (3.37 eV) the ZnO is emerging as a most suitable alternative of TiO_2 (Straumal et al., 2010; Rahman et al., 2013). In certain cases the ZnO exhibits higher photocatalytic activity and quantum efficiency than TiO_2. Moreover, in addition to photo-assisted reactions the ZnO is also used for anti-bacterial and self-cleaning activities (Mohd Yusof et al., 2019). Though, ZnO, TiO_2 and other comparable photo-catalyst under the UV-light have ability to degrade organic pollutant only. This happens because of photo-catalysts' wide band gap, which got activated only under UV-light irradiation. Therefore, on a broad scale the utilization of such photo-catalysts may results in low photo-electronic-transition efficiency as the UV-light consists only 4–5% of the solar spectrum. Thus, by considering the environmental pollution and energy conservation issues, it is essential to develop highly efficient visible light-driven photo-catalysts. Doping and nanocomposition of metal oxides have been considered as interesting way of modification. The doped metal oxides have shown excellent properties in photo-catalysis. Doping is the source of modification in the features and properties of nanomaterials. To meet the cumulative demands of various applications the nanocomposition and doping generally play an important role to improve the various properties of nanomaterials (metal oxides). These properties include size reduction and surface area enhancement of nanostructured metal oxides. Moreover, the tuning of bandgap-energy and shifting of absorption in the visible region through nanocomposition and doping enhances the solar photocatalytic properties (Asif et al., 2015; Asif et al., 2014).

As an efficient material for wastewater/water treatment iron (II) oxide (FeO) is very attractive due to low cost, easy availability, low or no-toxicity and hydrophilic nature. The FeO nanoparticles are used as efficient catalyst and heavy metal ions sorbent with excellent anti-viral and anti-bacterial activities (Lakhotia et al., 2019). Due to its unique optoelectronic, optical and magnet properties and wide industrial applications the Sb_2O_3 is very attractive semiconductor for researchers. The researchers used TiO_2 coupled Sb_2O_3 to expedite the photo-catalytic process. By doping with oxide electrodes the Sb_2O_3 is used to degrade the carbamazepine by photo-catalytic process (Kim et al., 2012; Wang et al., 2018).

Inspired from the current trend of the research, novel ternary composites of the oxides of different metals have prepared with the aim of testing of their photocatalytic properties. During this study the mixed-oxides of zinc-iron-calcium (ZnFeCa), zinc-iron-antimony (ZnFeSb), zinc-iron-titanium (ZnFeTi) and zinc-iron-cobalt (ZnFeCo) have been synthesized. The synthesized four different mixed-oxide compounds were characterized by XRD, XPS, SEM and EDS. Furthermore, all the prepared compounds were used more efficiently for the photocatalytic purification of wastewater by the degradation of the different dissolved dyes.

2. Experimental

2.1. Materials

The required lab grade materials and chemicals such as zinc chloride ($ZnCl_2$), iron chloride ($FeCl_3$), calcium chloride ($Cacl_2$), antimony chloride ($SbCl_3$), cobalt chloride ($CoCl_2$) and titanium dioxide were acquired from Sigma Aldrich. The required dyes such as acridine orange (AO), congo red (CR), brilliant green (BG), malachite green (MG) and methyl orange (MO) were acquired from BDH chemicals, England. The chemical formulae of AO, MG, BG, MO and CR are $C_{17}H_{19}N_3$, $C_{23}H_{25}N_2$, $C_{27}H_{33}N_2.HO_4S$, $C_{14}H_{14}N_3NaO_3S$ and $C_{32}H_{22}N_6Na_2O_6S_2$, respectively. Titanium dioxide (TiO_2) powder in anatase form with particle size < 25 nm was purchased from Sigma Aldrich. For aqueous solution preparation the distilled water was obtained from water Millipore-Q purification system in our lab.

2.2. Research methodology

2.2.1. Mixed metal-oxides synthesis

Initially, 0.1 M solution of zinc chloride ($ZnCl_2$), iron chloride ($FeCl_3$) and calcium chloride ($Cacl_2$) or antimony chloride ($SbCl_3$) or cobalt chloride ($CoCl_2$) were prepared in distilled water. Four zinc and iron-based oxide mixtures were synthesized by mixing equal quantities (1:1:1) of zinc chloride ($ZnCl_2$), iron chloride ($FeCl_3$) and calcium chloride ($Cacl_2$) or antimony chloride ($SbCl_3$) or titanium oxide (TiO_2) or cobalt chloride ($CoCl_2$) in distilled water. Then 0.1 M NaOH solution was added, and the solutions were kept at 50 to 60 °C and stirred overnight, while the pH was maintained around of 10 by using NaOH solution. Resultantly, the precipitates were obtained, which were washed with water and ethanol several times and then dried and ground. The obtained nanopowders were the mixtures of1: Zn, Fe and Ca oxides; 2: Zn, Fe and Sb oxides; 3: Zn, Fe and Ti oxides and 4: Zn, Fe and Co oxides.

2.2.2. Material characterization

The synthesized nanopowders were characterized by using Field Emission Scanning Electron Microscope (FESEM), X-ray diffractometer (XRD), energy-dispersive spectroscope (EDS) and X-ray photoelectron spectroscopy (XPS). The size and the morphology of the nanoparticles was analyzed by the FESEM (JEOL JSM 7600F Japan). For the chemical and crystal structure analysis the EDS (Oxford EDS system), XRD (PANalytical diffractometer) and XPS (Thermo Scientific k-α11066) were used. The synthesized

nanopowders were applied for the degradation of various dyes under sunlight.

2.2.3. Application of synthesized materials for dye degradation

For photocatalytic degradation study the 0.063 mM, 0.05 mM, 0.022 mM, 0.05 mM and 0.05 mM solutions of AO, MG, BG, MO and CR dyes were prepared, respectively in distilled water. Initially, all synthesized nanopowders were applied one by one for the degradation of acridine orange dye and the best nanomaterial was selected, which was then applied for the degradation of other dyes. All the experiments were carried out under the sun light. The effect of concentration of catalyst, pH of solution and light on the reaction rate were studied. The selected dye's solutions were prepared in various types of water samples and treated with selected catalyst (nanomaterial). These water samples were taken from sea, hospital waste, sanitary water and irrigation water. Moreover, two types of filters (tube type and funnel type) were prepared by using glass tube/funnel, cotton swab and the nanomaterial. The filters were used for the purification of polluted water samples. Before UV–visible spectroscopy, the photocatalyst was separated from the water sample by centrifugation. The UV–visible spectrophotometer (Thermo Scientific Evolution 300) was used for the measurement and monitoring of pollutants concentration and degradation. Throughout the experiments the quartz cuvettes were used as a reaction vessel.

3. Results and discussion

3.1. Analysis of mixed metal-oxides

3.1.1. Elemental and morphological characterization

The synthesized nanomaterials were characterized for chemical analysis by EDS. The EDS spectra of mixed-oxides of Zn-Fe-Ca, Zn-Fe-Sb, Zn-Fe-Ti and Zn-Fe-Co are shown in Fig. 1a, 1b, 1c and 1d, respectively. The spectra of the Fig. 1 confirm the presence of all constituting elements of the prepared oxides. The morphology and the sizes of the nanoparticles were analyzed by FESEM. Fig. 2a and 2c show FESEM images of the mixed oxides of Zn-Fe-Ca and Zn-Fe-Ti, respectively, that the nanoparticles are spherical in shape with 10 ± 5 nm diameter. The FESEM image of Zn-Fe-Sb mixed-oxides is shown in Fig. 2b. It can be seen that powder consists of rectangular particles of average size 20 ± 10 nm. The mixed oxides of Zn-Fe-Co consist of 10 ± 3 nm thick and 100 nm to 200 nm long flakes type particles that can be clearly seen in Fig. 2d. As all the oxide composites were prepared through same process in same conditions (pH and temperature) by keeping two reagents (ZnCl2 and FeCl3) same. Only one reagent in each sample was changed. So, it seems that the presence of Co is responsible for the crystallization of Zn-Fe-Co oxides in nano-flakes. Moreover, the synthesis process highly influences the structural morphology of nanoparticles (Wang et al., 2005; Yang et al., 2009; Sabry et al., 2020).

3.1.2. Crystal structure

The Fig. 3 shows the XRD-spectra of the synthesized oxides mixtures. The analysis was done by using PANalytical X-ray diffractometer by Cu Kα radiation of λ = 0.45 nm. The XRD operation was carried out at 50 mA and 40 KV, while the scan rate was fixed at 2° 2θ min^{-1}. The XRD patterns confirm the presence of synthesized oxides (Wang et al., 2018; Ahmad et al., 2016; Gardy et al., 2017; Rahman et al., 2018; Rahman et al., 2014).

3.1.3. XPS analysis

The XPS analysis of the synthesized mixed-oxides was done to find out the binding energies of Zn. Fe, Ca, Sb, Ti, Co and O by using K-Alpha 11066 spectrometer (Thermo Scientific) with Al K-α exciting radiation source, 400 μm beam spot size, 200.0 eV pass energy, 1.0 eV energy step size and ~8–10 Torr vacuum. The Fig. 4 shows the results of XPS analysis and the results are similar to the already reported results (Ahmad et al., 2016; Gardy et al., 2017; Rahman et al., 2018; Rahman et al., 2014). These results reveal the formation of ZnO, FeO, CaO, Sb_2O_3, TiO_2 and CoO. The binding energergies of ZnFeCa, ZnFeSb, ZnFeTi, and ZnFeCo were understood by XPS to appraise the mixed oxides' composition (Fig. 4). XPS spectrum of all mixed oxides depicted strong peaks for Fe, O, Zn along with their ternary element such as Ca in ZnFeCa, Sb in ZnFeSb, Ti in ZnFeTi, and Co in ZnFeCo. Substantial signals of O, Fe and Zn elements are presented in all the oxides spectra. A core level spectrum (magnified) of the Fe 2p and the Zn 2p are presented in Fig. 4(a) and Fig. 4(b), respectively, and each of them shows two peaks. The peaks existed at 726.1 and 712.3 eV in all the spectra are assigned to Fe 2p1/2 and Fe 2p3/2 while the peaks of Zn 2p existed at 1046.8 and 1023.6 eV are related to Zn 2p1/2 and Zn 2p3/2. Likewise, the peak at 531.2 eV depicts O 1s. Additionally, Ca, Sb, Ti and

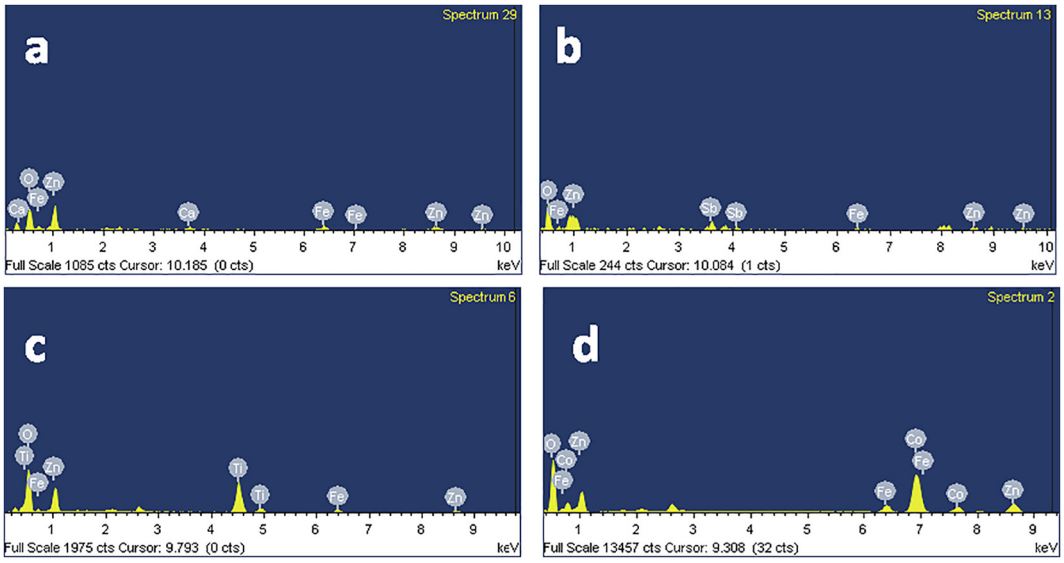

Fig. 1. EDS spectra of the mixed-oxides of (a) zinc-iron-calcium (ZnFeCa), (b) zinc-iron-antimony (ZnFeSb), (c) zinc-iron-titanium (ZnFeTi) and (d) zinc-iron-cobalt (ZnFeCo).

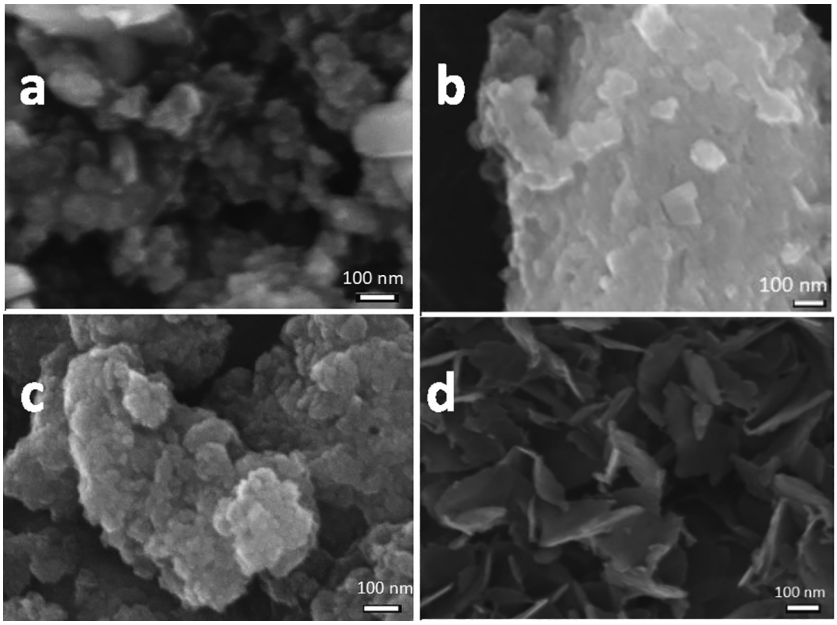

Fig. 2. FESEM images of the mixed-oxides of (a) zinc-iron-calcium (ZnFeCa), (b) zinc-iron-antimony (ZnFeSb), (c) zinc-iron-titanium (ZnFeTi) and (d) zinc-iron-cobalt (ZnFeCo).

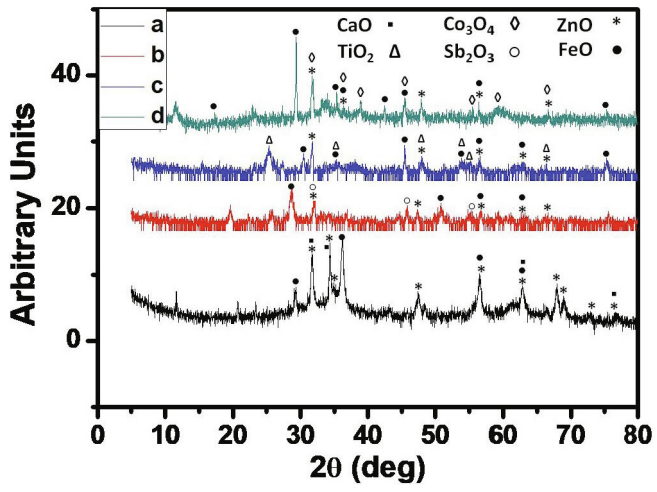

Fig. 3. X-ray diffraction patterns of mixed-oxides of (a) zinc-iron-calcium (ZnFeCa), (b) zinc-iron-antimony (ZnFeSb), (c) zinc-iron-titanium (ZnFeTi) and (d) zinc-iron-cobalt (ZnFeCo).

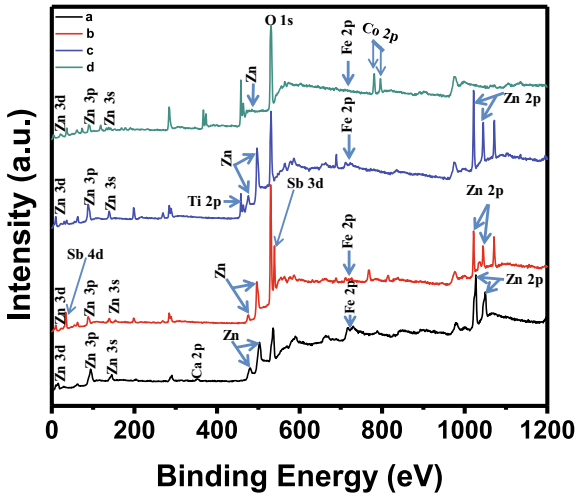

Fig. 4. XPS analysis of mixed-oxides of (a) zinc-iron-calcium (ZnFeCa), (b) zinc-iron-antimony (ZnFeSb), (c) zinc-iron-titanium (ZnFeTi) and (d) zinc-iron-cobalt (ZnFeCo).

Co peaks appeared at 352.1, 33.9, 458.2 and, 780.5 and 796.1 eV in ZnFeCa, ZnFeSb, ZnFeTi, and ZnFeCo, respectively.

3.2. Characterization of materials for water purification

AO is nitrogen containing heterocyclic dye that extensively used for the printing, leather dyeing, lithography and biological stains. It is also indicated by toxicological investigations that the aminoacridine has a mutagenic potential (Kasinathan et al., 2016). For our investigations we prepared a 0.0625 mM aqueous solution of AO in distilled water. From the prepared solution 3 to 3.5 ml solution was taken in to the quartz cuvette. To observe the absorbance of the dye the cuvette was put in to the UV–visible spectrophotometer. For the pollutant degradation we used the prepared mixed-oxides nanopowders. By putting the nanopowder in the solution (50 mg/50 ml of solution) in the presence of sunlight the dye degradation processes started which results in the color change of solution. The degradation of dye was evaluated by taking samples after a specific interval of time. The performance of the oxide complexes for pollutant degradation was calculated by using the following formula (Ali et al., 2018):

$$\text{Percentage Degradation} = \frac{A_0 - A_i}{A_0} x100 \quad (1)$$

where, A_0 represents dye's initial absorbance at λ_{max} and the A_i is the absorbance of dye at an instantaneous interval of time. Same procedure was adopted for all other dyes (pollutant) such as MG, BG, MO and CR and the results were compared for optimization.

The UV–visible spectra of acridine orange (AO) dye reduction as a function of time in the presence of solar light and the mixed-oxides of ZnFeCa, ZnFeSb, ZnFeTi and ZnFeCo are shown in Fig. 5a, 5b, 5c and 5d, respectively. The fastest 98% degradation

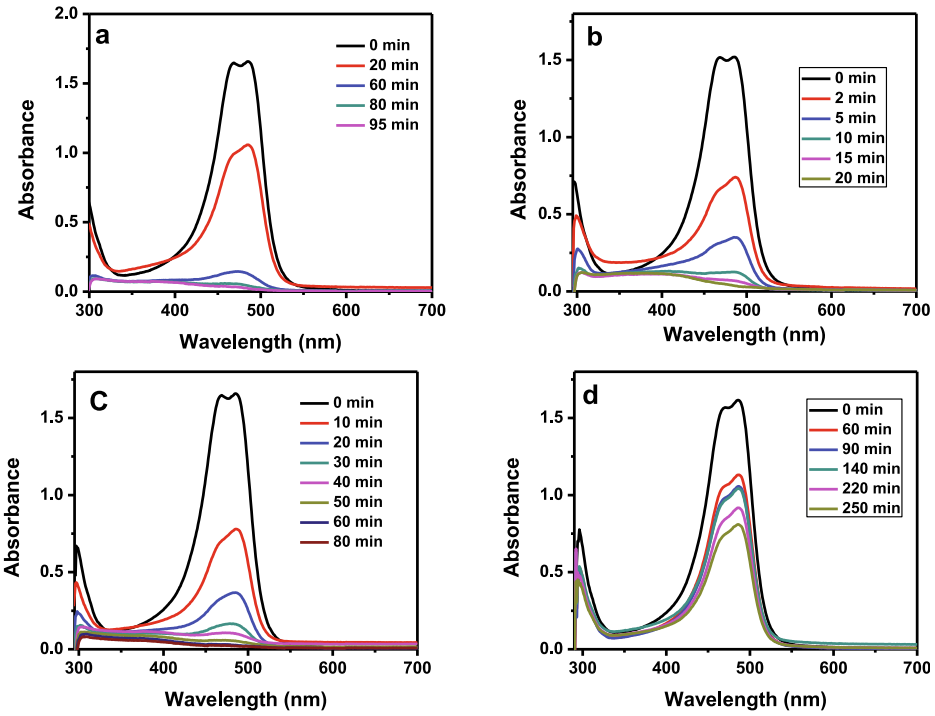

Fig. 5. UV–visible spectra of AO dye reduction as a function of time in the presence of solar light and the mixed-oxides of (a) ZnFeCa (b) ZnFeSb (c) ZnFeTi and (d) ZnFeCo.

of AO dye was observed in the case of mixed-oxides of ZnFeSb within 20 min, while the same level of degradation was attained within 95 min and 80 min, respectively with mixed-oxides of ZnFeCa and ZnFeTi. Moreover, only 51 % dye degradation was observed in 250 min while using ZnFeCo mixed-oxide. The percentage degradation of AO dye versus time in the presence of oxide complexes and sunlight is shown Fig. 6. It is evident from the Fig. 6 that within 20 min only 36 % and 78 % degradation take place in case of ZnFeCa and ZnFeTi mixed-oxides. As the oxides of ZnFeSb showed a best performance for the degradation of pollutant (dye) as compared to equal amounts of other catalysts, so, it was further investigated for various water pollutants (dyes).

Fig. 7a, 7b, 7c, 7d and 7e, respectively show the UV–visible spectra of AO, MG, BG, MO and CR dyes reduction from the aqueous solutions as a function of time in the presence of solar light and

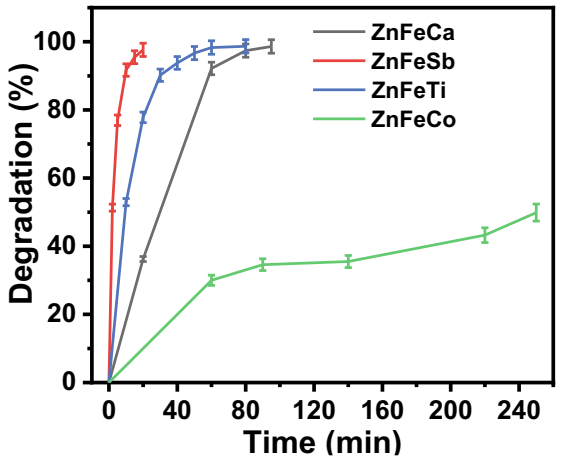

Fig. 6. Percentage degradation of AO dye versus time in the presence of mixed-oxides nanopowders and sunlight.

the ZnFeSb mixed-oxides. Fig. 7 shows that the AO, MG and BG dyes reduced by up to 98 %, 94 % and 96 % within 20 min, 145 min and 70 min, respectively while the reduction of MO and CR dyes is very small. As the concentration of dye in the aqueous solution of AO (0.0625 mM) is high as compared to MG (0.05 mM) and BG (0.022 mM) and it takes minimum time (20 min) for maximum degradation (98 %), so the AO dye was selected for further investigation. The comparison of dyes degradation from their aqueous solutions within 20 min is shown in Fig. 7f. It is obvious that ZnFeSb is more selective for AO, which might be due to the surface charges and morphology of ZnFeSb that are more suitable for the degradation of AO. ZnFeSb surface especially at high pH is negative, while AO is cationic; thus there is high interaction between AO and ZnFeSb. Hence, it shows high degradation and high selectivity toward AO.

As the amount of catalyst is very important in photo-catalysis, the effect of catalyst concentration on the reaction rate was also studied. For the optimization, five different amounts (0.2 mg/ml to 1.0 mg/ml with increment of 0.2 mg/ml) of catalysts (Zn-Fe-Sb mixed-oxides) were used for the degradation of pollutant (dye) from the 0.0625 mM aqueous solution of AO. The percentage degradation-catalyst concentration relationship for AO dye solution and Zn-Fe-Sb mixed-oxides in the presence of sunlight for 20 min is shown in Fig. 8. The graph (Fig. 8) shows that with increase in amount of catalyst the photocatalytic reaction speeds up. When the concentration was 0.2 mg/ml the reaction time was 120 min but on increasing catalyst's concentration up to 1.0 mg/ ml the reaction time reduced to only 20 min. So, this amount (1.0 mg/ml) was selected for further investigations.

The effect of light on the reaction time was also studied. For the catalytic degradation of pollutant from AO dye (0.0625 mM) aqueous solution two types of light (solar light and artificial light) were used in the presence of Zn-Fe-Sb mixed-oxides (catalyst). The source of artificial light was 400-watt filament bulb. During reaction no stirring was done. Fig. 9 gives the comparison of the light sources to complete the degradation process. The Fig. 9 shows that

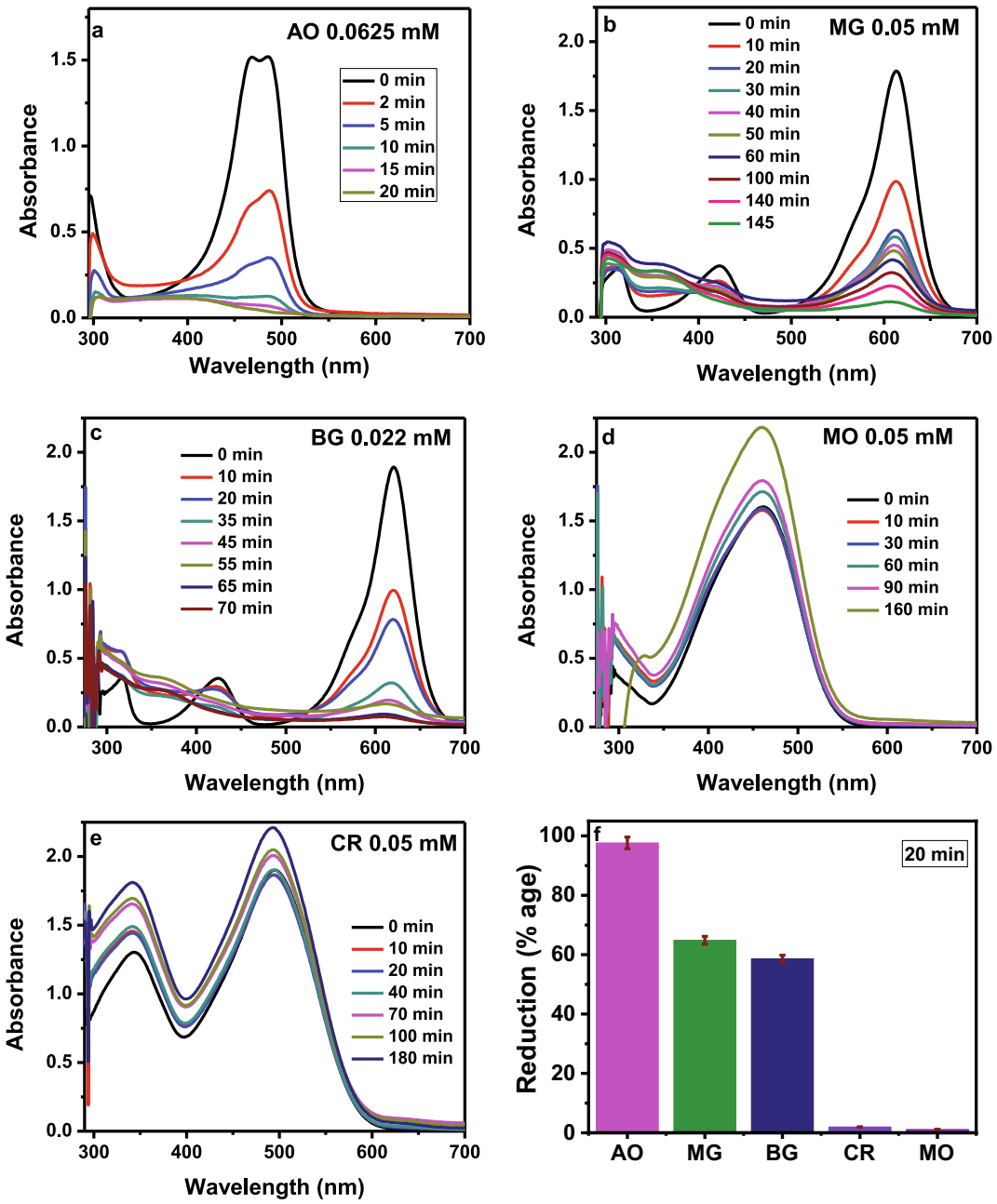

Fig. 7. The UV–visible spectra of AO (a), MG (b), BG (c), MO (d) and CR (e) dyes reduction from the aqueous solutions as a function of time in the presence of solar light and the ZnFeSb oxides and the comparison of dyes degradation (f).

sunlight is more effective as compared to the artificial light. So, the use sunlight was continued to further investigations.

The effect of pH on the degradation process was studied. For this purpose, the pH of 0.0625 mM AO dye solution was decreased or increased by adding drops of acidic or basic solutions. Seven solutions with different pH (pH 3 to pH 8 with increment of 1 and pH 11) were prepared and their initial absorbance was studied. It was found that the decrease in pH (7 to 3) of solution had no significant effect on the initial absorbance of solution but on increasing the pH the initial absorbance decreased abruptly as shown in the Fig. 10a. The Fig. 10b, 10c and 10d show the degradation behavior of AO dye solutions of various pH in the presence of Zn-Fe-Sb mixed-oxides and sunlight. AO has cationic properties and in acidic medium, the surface of ZnFeSb surface will show positive charge while in alkaline medium, its surface will be negatively charged. Cationic nature of AO dye favor higher adsorption on the negatively charged ZnFeSb surface at high pH due to the fact that electrostatic interactions between ZnFeSb– and AO+ dominate. Hence, high approach of AO on the ZnFeSb surface with increase in pH of solution and therefore it shows high degradation at high pH.

We focused on the solutions of pH 3 to pH7. The effect of pH on the degradation behavior of AO dye solution is shown in Fig. 11. The reaction rate increases with increase in pH up to pH 7. The maximum reaction rate was observed in the solution of pH 7. Therefore, solution of pH seven is considered best for the Zn-Fe-Sb mixed-oxides catalyst. The comparison of present work with the already reported literature is given in Table 1.

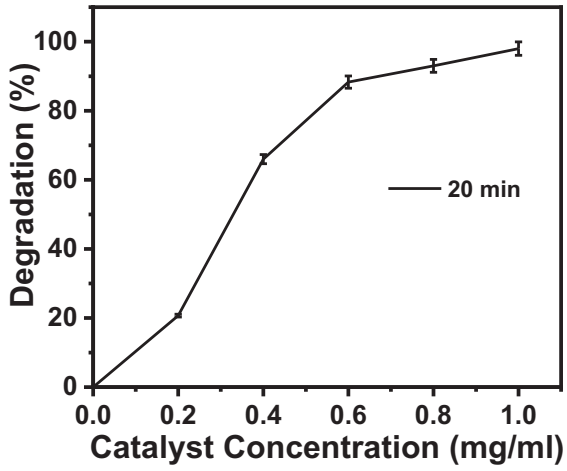

Fig. 8. Percentage degradation-catalyst concentration relationship for the AO dye solution and Zn-Fe-Sb mixed-oxides in the presence of sunlight.

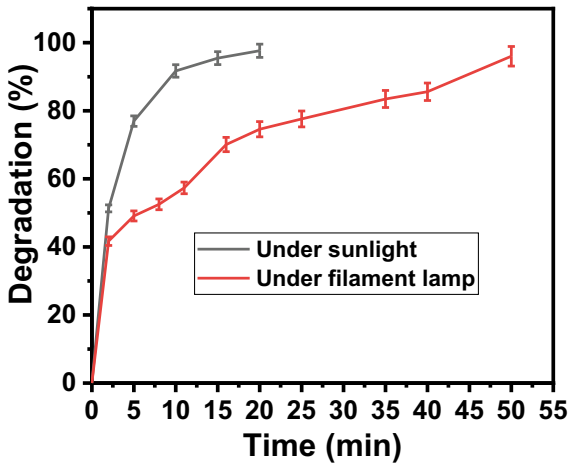

Fig. 9. Effect of light on the degradation behavior of AO dye solution in the presence of Zn-Fe-Sb mixed-oxides.

The selected mixed-oxides of Zn-Fe-Sb were applied to remove AO dye (pollutant) from various types of water. For this purpose, water samples were taken from four different sources. The tap water was taken from the chemistry lab of King Abdulaziz University, Jeddah, distilled water was also taken from the Millipore-Q water purification system in Chemistry lab of King Abdulaziz University, Jeddah and the seawater sample was taken from the Red Sea, while the SBR is the sewage wastewater of Buraiman area of Jeddah. The AO dye was added to the water sample to make the solutions of almost same concentration (0.0625 mM). To study the dye degradation behavior of various water samples, the nanocatalyst (Zn-Fe-Sb mixed-oxides) was added (1.0 mg/ml) in the presence of sunlight. The Fig. 12 shows the degradation behavior of the AO dye in various water samples. Fig. 12 shows that fastest degradation occurred in DI water (20 min) and then respectively in tap water (70 min), SBR water (85 min) and sea water (120 min). This delay in degradation process may be due to presence of various elements.

For water purification two types of filters were designed; one is tube type and the other is funnel type (Fig. 13a and 13b). The tube type filter consists of a glass tube, which is opened on both ends but on one end is converged and makes narrow opening. To make a water filter the cotton swab of 5 mm height was inserted in the converged end, on the cotton swab about 3 mm layer of catalyst (Zn-Fe-Sb mixed oxides) nanopowder was applied. The tube type water filter is shown in Fig. 13a. The polluted water is poured in to the tube through open end, which passes through the catalyst in the presence of sunlight and the purification process occurs and the pure water is obtained from the narrow end which is collected in sample tube/glass beaker. This filter works under the sunlight. The 0.0625 mM solution of AO dye was filtered through the tube type filter, in only one pass the fully cleaned water was obtained as a filtrate, which was analyzed by UV–visible photospectrometer and the results are shown in Fig. 13c. The Fig. 13c shows that filter works very well and in only one pass the dye degrades completely (almost 99 % degradation).

The second type of filter is funnel type filter. Its structure is same as tube type filter but instead of tube glass funnel is used. The cotton swab is inserted in stem of funnel; on the top of cotton swab the layer of catalyst nanopowder is applied. The polluted water is poured in to the mouth of funnel and it passes through the filter in the stem to give clean water as a filtrate. The funnel type filter is shown in Fig. 13b. The UV–visible spectra of aqueous solution of AO dye before and after filtration though funnel type filter is shown in Fig. 13d. After one pass through the filter in the presence of solar light the dye was degraded completely.

The mechanism of photo-degradation is based on transformation of organic dyes (pollutants) into gaseous carbon dioxide (CO_2), ammonium, nitrate and sulfate ions. Schematic representation of the general photocatalytic degradation process of organic pollutant is the following (Azeez et al., 2018; Chadwick et al., 2002):

a. On the absorption of photon of sufficient energy into the surface of metal oxide (MO) the valance electron migrates from valance to conduction band and caused to generate the electron and hole in the conduction and valance band, respectively

$$MO + h\nu \rightarrow e^{-}_{CB} + h^{+}_{VB} \quad (2)$$

b. On the surface of catalyst, the physically adsorbed oxygen undergoes ionosorption by taking electron

$$(O_2)_{ads} + e^{-}_{CB} \rightarrow O_2^{-} \quad (3)$$

c. Production of OH· radicals by neutralizing the hydroxyl group (OH^{-}) with photo-holes

$$(H_2O \leftrightarrow OH^{-} + H^{+}) + h^{+}_{VB} \rightarrow OH^{\cdot} + H^{+} \quad (4)$$

d. Neutralization of O^{-}· by proton

$$H^{+} + O_2^{-\cdot} \rightarrow HO_2^{\cdot} \quad (5)$$

e. Formation of hydrogen peroxide (transient) and mutation of oxygen

$$2HO_2^{\cdot} \rightarrow O_2 + H_2O_2 \quad (6)$$

f. Hydrogen peroxide decomposition and reduction of oxygen

$$H_2O_2 \rightarrow OH^{-} + OH^{\cdot} \quad (7)$$

g. OH· causes to oxidize pollutant (organic reactant)

$$OH^{\cdot} + R \rightarrow OH + R^{\cdot} \quad (8)$$

h. Organic pollutant also directly oxidized by the holes

$$R + h^{+}_{VB} \rightarrow R^{+\cdot} \rightarrow \text{degradation products} \quad (9)$$

4. Conclusions

During this study nanopowders of four different mixed-oxides were synthesized successfully by using low temperature synthesis method. Out of these four mixed-oxides, three showed good catal-

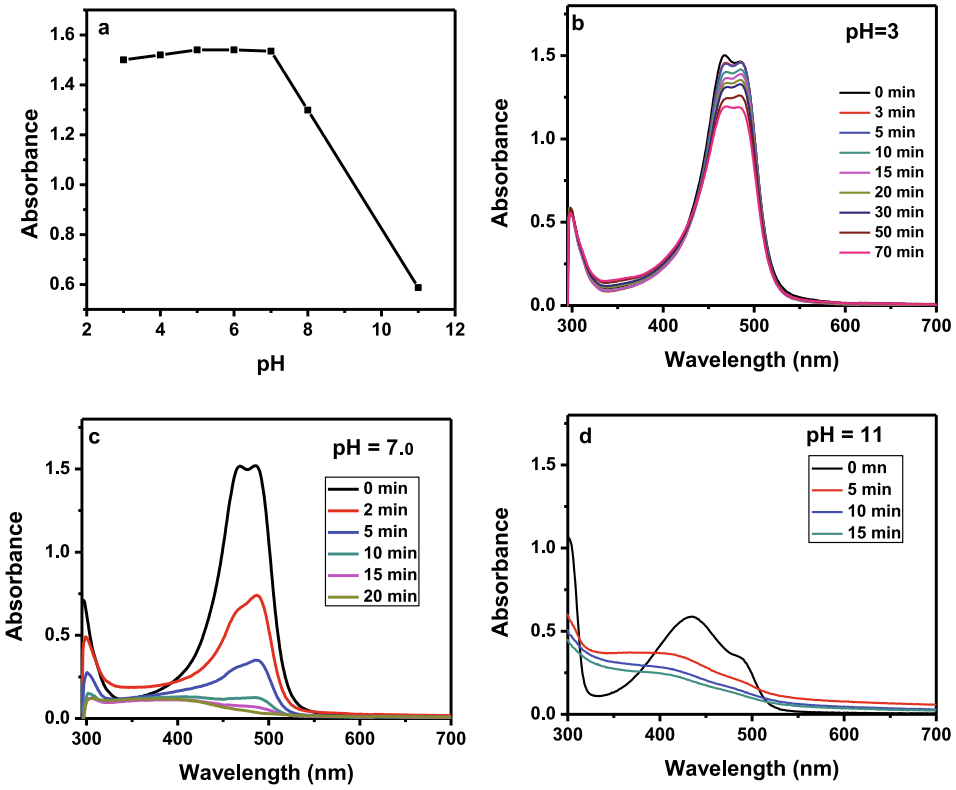

Fig. 10. Effect of pH on the initial absorbance of the aqueous solution of AO dye (a) and the degradation behaviors of solutions of pH 3 (b), pH 7 (c) and pH 11 (d).

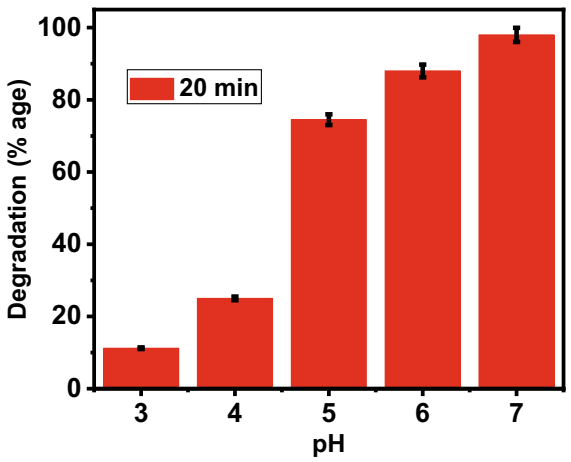

Fig. 11. Effect of pH on the degradation behavior of AO dye solution in the presence of Zn-Fe-Sb mixed-oxides and sunlight.

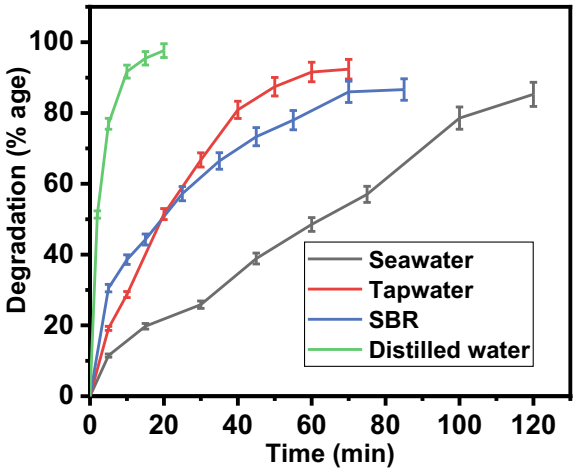

Fig. 12. Pollutant (dye) degradation behavior from the various water samples.

Table 1
Comparison of various nanoparticles for the photolytic degradation of acridine orange dye (AO).

Sr. No	Catalyst	Catalyst dosage (mg/ml)	Dye Conc. (mM)	Degradation (% age)	Time (min)	Light source	Refs.
1	CuS NPs	0.5	0.037	45	180	UV	Siddique et al. (2018)
2	ZnO NPs	5.0	0.02	92.8	150	500 W HL	Pare et al. (2008)
3	Silica NPs	3.33	0.01	58	50	UV/Vis	Selvaggi et al. (2015)
4	TiO2 (anatase) NPs	10	0.04	97	402	UV	Zubieta et al. (2012)
5	TiO2 (rutile) NPs	10	0.04	67	480	UV	Amini and Ashrafi (2016)
6	ZnO NPS	1.0	0.037	98	50	SL	Amini and Ashrafi (2016)
7	$Nd_{0.3}Sr_{0.7}MnO_3$	0.5	0.03	95	180	Vis	Abdel-Latif et al. (2019)
8	Ce-Sr oxide	1.0	0.03	90	180	Vis	Arshad et al. (2017)
9	Ce-Cd oxide	1.0	0.03	90	180	Vis	Arshad et al. (2017)
10	ZnFeSb oxides	1.0	0.063	98	20	Sunlight	Current Study

NP: Nanoparticles, HL: Halogen lamp, UV: Ultraviolet light, Vis: Visible light, SL: Solar light.

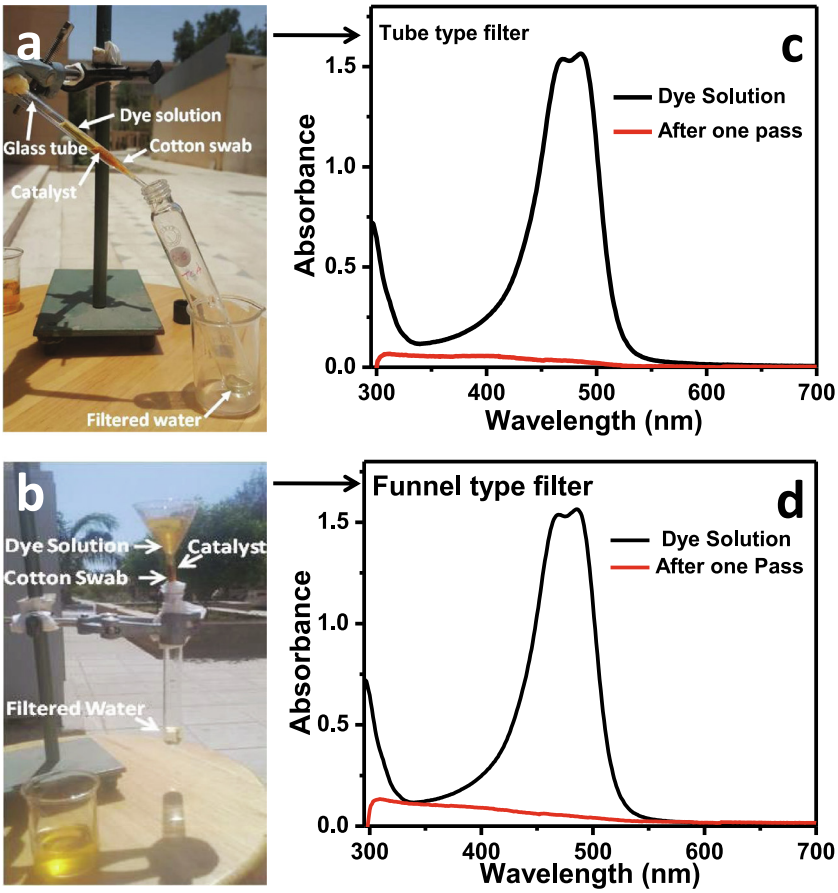

Fig. 13. Tube type (a) and funnel type (b) filters for water purification and the UV–visible spectra of aqueous solution of AO dye before and after filtration through tube type (c) and funnel type (d) filters.

ysis behavior for AO dye degradation under the sunlight (solar energy), but only one mixed-oxide (Zn-Fe-Sb) were selected for detailed investigation because Zn-Fe-Sb mixed-oxides showed the fastest 98% degradation of AO dye within 20 min. Further, Zn-Fe-Sb showed better performance under sunlight (solar energy) as compared to filament light. The selected mixed-oxides (Zn-Fe-Sb) are effective for the degradation of MG and BG dyes dissolved in water but more efficient for AO dye. For the AO dye degradation, the most favorable conditions are pH 7, sunlight and 1.0 mg/ml catalyst concentration. The Zn-Fe-Sb mixed-oxides based water filters showed best performance for water purification under sunlight and removed up to 99 % dye content in one pass. Based on the experimental results it may be expected that the synthesized catalysts nanomaterials are fascinating for commercialization as they utilized the sunlight (free and abundant source of energy) for wastewater treatment.

5. Compliance with ethical standards

Not applicable.

Conflict of interest statement

The author declare that he has no known competing financial interests or personal relationships that could have appeared to influence the work reported in this paper.

Declaration of Competing Interest

The authors declare that they have no known competing financial interests or personal relationships that could have appeared to influence the work reported in this paper.

Acknowledgements

This project was funded by the KAU Endowment (WAQF) at King Abdulaziz University Jeddah, Saudi Arabia. The authors, therefore, acknowledge with thanks KAU Endowment (WAQF) for technical and financial support.

References

Ong, Y.T., Ahmad, A.L., Zein, S.H.S., Tan, S.H., 2010. A review on carbon nanotubes in an environmental protection and green engineering perspective. Braz. J. Chem. Eng. 27, 227–242.
Rajasulochana, P., Preethy, V., 2016. Comparison on efficiency of various techniques in treatment of waste and sewage water–A comprehensive review. Resour.-Effic. Technol.
Savage, N., Diallo, M.S., 2005. Nanomaterials and water purification: opportunities and challenges. J. Nanopart. Res. 7, 331–342.
Rajeev, B., Yesodharan, S., Yesodharan, E., 2015. Application of solar energy in wastewater treatment: photocatalytic degradation of α-methylstyrene in water in presence of ZnO. J. Water Process Eng. 8, 108–118.
Rauf, M., Ashraf, S.S., 2009. Fundamental principles and application of heterogeneous photocatalytic degradation of dyes in solution. Chem. Eng. J. 151, 10–18.
Matthews, R.W., 1986. Photo-oxidation of organic material in aqueous suspensions of titanium dioxide. Water Res. 20, 569–578.

Lu, M., Pichat, P., 2013. Photocatalysis and Water Purification: from Fundamentals to Recent Applications. John Wiley & Sons.
Ollis, D., Pichat, P., Serpone, N., 2010. TiO 2 photocatalysis-25 years. Appl. Catal. B 99, 377.
Ali, N., Awais, Kamal, T., Ul-Islam, M., Khan, A., Shah, S.J., Zada, A., 2018. Chitosan-coated cotton cloth supported copper nanoparticles for toxic dye reduction. Int. J. Biol. Macromol. 111, 832–838.
Kamal, T., Ahmad, I., Khan, S.B., Asiri, A.M., 2019. Bacterial cellulose as support for biopolymer stabilized catalytic cobalt nanoparticles. Int. J. Biol. Macromol. 135, 1162–1170.
Khan, M.S.J., Kamal, T., Ali, F., Asiri, A.M., Khan, S.B., 2019. Chitosan-coated polyurethane sponge supported metal nanoparticles for catalytic reduction of organic pollutants. Int. J. Biol. Macromol. 132, 772–783.
Khan, M.S.J., Khan, S.B., Kamal, T., Asiri, A.M., 2019. Agarose biopolymer coating on polyurethane sponge as host for catalytic silver metal nanoparticles. Polym. Test. 78, 10.
Ali, F., Khan, S.B., Kamal, T., Alamry, K.A., Asiri, A.M., 2018. Chitosan-titanium oxide fibers supported zero-valent nanoparticles: highly efficient and easily retrievable catalyst for the removal of organic pollutants. Sci. Rep. 8, 6260.
Kasinathan, K., Kennedy, J., Elayaperumal, M., Henini, M., Malik, M., 2016. Photodegradation of organic pollutants RhB dye using UV simulated sunlight on ceria based TiO2 nanomaterials for antibacterial applications. Sci. Rep. 6, 38064.
Kaviyarasu, K., Maria Magdalane, C., Jayakumar, D., Samson, Y., Bashir, A.K.H., Maaza, M., Letsholathebe, D., Mahmoud, A.H., Kennedy, J., 2020. High performance of pyrochlore like Sm2Ti2O7 heterojunction photocatalyst for efficient degradation of rhodamine-B dye with waste water under visible light irradiation. J. King Saud Univ. – Sci. 32, 1516–1522.
Rathnakumar, S.S., Noluthando, K., Kulandaiswamy, A.J., Rayappan, J.B.B., Kasinathan, K., Kennedy, J., Maaza, M., 2019. Stalling behaviour of chloride ions: a non-enzymatic electrochemical detection of α-Endosulfan using CuO interface. Sens. Actuators, B 293, 100–106.
Panimalar, S., Uthrakumar, R., Selvi, E.T., Gomathy, P., Inmozhi, C., Kaviyarasu, K., Kennedy, J., 2020. Studies of MnO2/g-C3N4 hetrostructure efficient of visible light photocatalyst for pollutants degradation by sol-gel technique. Surf. Interfaces 20, 100512.
Khan, S.A., Khan, S.B., Asiri, A.M., 2016. Toward the design of Zn–Al and Zn–Cr LDH wrapped in activated carbon for the solar assisted de-coloration of organic dyes. RSC Adv. 6, 83196–83208.
Khan, I., Saeed, K., Khan, I., 2019. Nanoparticles: properties, applications and toxicities. Arabian J. Chem. 12, 908–931.
Cheng, H., Wang, J., Zhao, Y., Han, X., 2014. Effect of phase composition, morphology, and specific surface area on the photocatalytic activity of TiO2 nanomaterials. RSC Adv. 4, 47031–47038.
Ali, F., Khan, S.B., Kamal, T., Anwar, Y., Alamry, K.A., Asiri, A.M., 2017. Anti-bacterial chitosan/zinc phthalocyanine fibers supported metallic and bimetallic nanoparticles for the removal of organic pollutants. Carbohydr. Polym. 173, 676–689.
Kamal, T., Ahmad, I., Khan, S.B., Ul-Islam, M., Asiri, A.M., 2019. Microwave assisted synthesis and carboxymethyl cellulose stabilized copper nanoparticles on bacterial cellulose nanofibers support for pollutants degradation. J. Polym. Environ. 27, 2867–2877.
Rahman, Q.I., Ahmad, M., Mehta, S., 2017. Hydrothermal synthesis of Cr-doped SrTiO 3 nanoparticles for rhodamine-B dye degradation under visible light illumination. Colloid Polym. Sci. 295, 933–937.
Lam, S.-M., Sin, J.-C., Abdullah, A.Z., Mohamed, A.R., 2012. Degradation of wastewaters containing organic dyes photocatalysed by zinc oxide: a review. Desalin. Water Treat. 41 (1-3), 131–169.
Pare, B., Jonnalagadda, S.B., Tomar, H., Singh, P., Bhagwat, V.W., 2008. ZnO assisted photocatalytic degradation of acridine orange in aqueous solution using visible irradiation. Desalination 232, 80–90.
Sakthivel, S., Neppolian, B., Shankar, M.V., Arabindoo, B., Palanichamy, M., Murugesan, V., 2003. Solar photocatalytic degradation of azo dye: comparison of photocatalytic efficiency of ZnO and TiO2. Sol. Energy Mater. Sol. Cells 77, 65–82.
Straumal, B., Protasova, S., Mazilkin, A., Myatiev, A., Straumal, P., Schütz, G., Goering, E., Baretzky, B., 2010. Ferromagnetic properties of the Mn-doped nanograined ZnO films. J. Appl. Phys. 108, 073923.
Rahman, Q.I., Ahmad, M., Misra, S.K., Lohani, M., 2013. Effective photocatalytic degradation of rhodamine B dye by ZnO nanoparticles. Mater. Lett. 91, 170–174.
Mohd Yusof, H., Mohamad, R., Zaidan, U.H., Abdul Rahman, N.A., 2019. Microbial synthesis of zinc oxide nanoparticles and their potential application as an antimicrobial agent and a feed supplement in animal industry: a review. J. Anim. Sci. Biotechnol. 10, 57.
Asif, S.A.B., Khan, S.B., Asiri, A.M., 2015. Visible light functioning photocatalyst based on Al2O3 doped Mn3O4 nanomaterial for the degradation of organic toxin. Nanoscale Res. Lett. 10, 355.
Asif, S.A.B., Khan, S.B., Asiri, A.M., 2014. Efficient solar photocatalyst based on cobalt oxide/iron oxide composite nanofibers for the detoxification of organic pollutants. Nanoscale Res. Lett. 9, 510.
Lakhotia, S.R., Mukhopadhyay, M., Kumari, P., 2019. Iron oxide (FeO) nanoparticles embedded thin-film nanocomposite nanofiltration (NF) membrane for water treatment. Sep. Purif. Technol. 211, 98–107.
Kim, H.W., Na, H.G., Bae, J., Yang, J.C., Kim, S.S., Cheong, H., Kim, D.Y., 2012. Synthesis and characterization of orthorhombic Sb2O4 nanowire prepared by heating Sb2S3 powder. Electrochem. Solid-State Lett. 15, K49–K52.
Wang, Z., Srivastava, V., Iftekhar, S., Ambat, I., Sillanpää, M., 2018. Fabrication of Sb2O3/PbO photocatalyst for the UV/PMS assisted degradation of carbamazepine from synthetic wastewater. Chem. Eng. J. 354, 663–671.
Wang, D., Song, C., Hu, Z., Zhou, X., 2005. Synthesis of silver nanoparticles with flake-like shapes. Mater. Lett. 59, 1760–1763.
Yang, X.i., Chen, Q.-W., Zhang, J.-Z., 2009. Shape-controlled synthesis and self-assembly of hexagonal cobalt ultrathin nanoflakes. Mater. Chem. Phys. 113, 675–679.
Sabry, R., Fikry, M., Ahmed, O.S., Zekri, A.R.N., Zedan, A.F., 2020. Laser-induced synthesis of pure zinc oxide nanoflakes. J. Phys. Conf. Ser. 1472, 012005.
Ahmad, R., Tripathy, N., Khan, M.Y., Bhat, K.S., Ahn, M.-S., Hahn, Y.-B., 2016. Ammonium ion detection in solution using vertically grown ZnO nanorod based field-effect transistor. RSC Adv. 6, 54836–54840.
Gardy, J., Hassanpour, A., Lai, X., Ahmed, M.H., Rehan, M., 2017. Biodiesel production from used cooking oil using a novel surface functionalised TiO2 nano-catalyst. Appl. Catal. B 207, 297–310.
Rahman, M.M., Alam, M.M., Asiri, A.M., 2018. Sensitive 1,2-dichlorobenzene chemi-sensor development based on solvothermally prepared FeO/CdO nanocubes for environmental safety. J. Ind. Eng. Chem. 62, 392–400.
Rahman, M.M., Khan, S.B., Asiri, A.M., Bhargava, S., 2014. Fabrication of smart chemical sensors based on transition-doped-semiconductor nanostructure materials with μ-chips. PLoS ONE 9 (1), e85036.
Siddique, F., Rafiq, M.A., Afsar, M.F., Hasan, M.M., Chaudhry, M.M., 2018. Enhancement of degradation of mordant orange, safranin-O and acridine orange by CuS nanoparticles in the presence of H 2 O 2 in dark and in ambient light. J. Mater. Sci.: Mater. Electron. 29, 19180–19191.
Selvaggi, R., Tarpani, L., Santuari, A., Giovagnoli, S., Latterini, L., 2015. Silica nanoparticles assisted photodegradation of acridine orange in aqueous suspensions. Appl. Catal. B 168-169, 363–369.
Zubieta, C.E., Messina, P.V., Schulz, P.C., 2012. Photocatalytic degradation of acridine dyes using anatase and rutile TiO2. J. Environ. Manage. 101, 1–6.
Amini, M., Ashrafi, M., 2016. Photocatalytic degradation of some organic dyes under solar light irradiation using TiO2 and ZnO nanoparticles. Nanochem. Res. 1, 79–86.
Abdel-Latif, I., Al-Hajji, L., Faisal, M., Ismail, A.A., 2019. Doping Strontium into neodymium Manganites nanocomposites for enhanced Visible light Driven photocatalysis. Sci. Rep. 9, 1–11.
Arshad, T., Khan, S.A., Faisal, M., Shah, Z., Akhtar, K., Asiri, A.M., Ismail, A.A., Alhogbi, B.G., Khan, S.B., 2017. Cerium based photocatalysts for the degradation of acridine orange in visible light. J. Mol. Liq. 241, 20–26.
Azeez, F., Al-Hetlani, E., Arafa, M., Abdelmonem, Y., Nazeer, A.A., Amin, M.O., Madkour, M., 2018. The effect of surface charge on photocatalytic degradation of methylene blue dye using chargeable titania nanoparticles. Sci. Rep. 8, 7104.
Chadwick, M., Goodwin, J., Lawson, E., Mills, P., Vincent, B., 2002. Surface charge properties of colloidal titanium dioxide in ethylene glycol and water. Colloids Surf., A 203, 229–236.